2007 IEEE International Conference on
Robotics and Automation
Roma, Italy, 10-14 April 2007

Polychaete-like Pedundulatory Robotic Locomotion

Michael Sfakiotakis, Dimitris P. Tsakiris and Kostas Karakasiliotis

Abstract— **The polychaete annelid marine worms propel themselves in a variety of challenging locomotion environments by a unique form of tail-to-head body undulations, combined with the synchronized action of numerous parapodial lateral appendages. This combined parapodial and undulatory mode of locomotion is termed *pedundulatory* in the present work. Robotic analogues of this type of locomotion are being studied, both in simulation, and via experiments with biomimetic robotic prototypes, which combine undulatory movements of their multi-link body with appropriately coordinated parapodial link oscillations. Extensive experimental studies of locomotion on sand demonstrate the potential of the pedundulatory robotic prototypes, especially their rich gait repertoire and their enhanced performance compared to robotic prototypes relying only on body undulations.**

Keywords - biomimetic robotics, undulatory locomotion, legged locomotion, motion control, polychaete annelids.

I. INTRODUCTION

Our previous work [1]–[3] has identified, and started replicating, an intriguing biological paradigm of locomotion in a variety of unstructured environments, namely that of the polychaete annelid segmented marine worms: they are living in the depths of the ocean, floating near the surface, or burrowing in the mud and sand of the seashore. Their adaptation to so diverse habitats impacts directly their morphology, sensory apparatus and nervous system structure (Fig. 1a). Their locomotion is characterized by the combination of a unique form of tail-to-head body undulations (opposite direction of propagation than snakes or eels), with the rowing-like action of their numerous active lateral appendages, called parapodia, distributed along their segmented body [4]–[6]. Robotic analogues of the polychaete tail-to-head body undulations were studied in [1], in the context of locomotion on sand. However, the combination of parapodial and undulatory locomotion, termed *pedundulatory* in the present work, merits special attention, as it provides these worms with distinctive locomotory modes, increasing their terrain traversing and manipulation capabilities. If properly replicated, it could benefit emerging robotic applications ranging from novel diagnostic systems for healthcare (e.g. endoscopic access to the human gastrointestinal tract) to robotic tools for search-and-rescue operations and to planetary exploration.

Robotic investigations of undulatory locomotion, has led mostly to wheeled mechanisms for terrestrial locomotion over relatively smooth surfaces (e.g., [7]–[11]). Recent innovative research efforts on non-wheeled undulatory locomotion bring forth the importance of understanding the interaction of the undulatory mechanism with the environment enabling the locomotion [1], [8], [12]–[16].

(a)

(b)

Fig. 1. (a) *Nereis virens*, a polychaete annelid marine worm. (b) The Nereisbot pedundulatory robotic prototype.

Drawing inspiration from the body plan and locomotion strategies of the polychaete annelids, we have developed several robotic prototypes, which combine body undulations with the paddle-like action of active lateral parapodial appendages. Sections II and III of the paper describe models of the mechanics and motion control of polychaete pedundulatory locomotion, and present associated simulation studies. Section IV describes the *Nereisbot* pedundulatory robotic prototype (Fig. 1b), which is capable of locomotion over unstructured substrates, and allows the validation and refinement of these models. The locomotory advantage of using parapodia to complement body undulations is demonstrated in Section V by robotic experiments of locomotion on sand, which also verify that our computational models capture adequately essential features of polychaete locomotion.

II. MODELING PEDUNDULATORY LOCOMOTION

The computational models developed to study the proposed locomotion strategy employ the SIMUUN simulation environment [17], which is based on the SimMechanics physical modeling toolbox of Matlab/Simulink.

A. Mechanism Model

Following the Nereisbot prototype design, the mechanism model contains five links (link-1 is the tail, and link-5 is the mechanism's head), interconnected by a total of four planar rotary joints J_i, whose actively-controlled joint angles are denoted by ϕ_i, while the distance between two consecutive joints is denoted by l (Fig. 2). Mounted on each of the first four segments, at a distance b from the segment's joint, are

This work was supported in part by the European Commission, through the IST projects MATHESIS (FP6-027574) and VECTOR (FP6-033970).

The authors are with the Institute of Computer Science, Foundation for Research & Technology – Hellas, Vassilika Vouton, P.O. Box 1385, Heraklion, Greece {sfakios,tsakiris}@ics.forth.gr

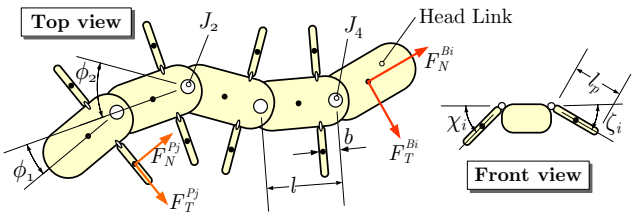

Fig. 2. Model of the Nereisbot prototype.

a pair of laterally placed parapodial links of length l_p. These are connected to the segment via planar dorso-ventrally oriented single-degree-of-freedom rotary joints, whose angles to the horizontal are denoted by χ_i and ζ_i. The system's equations of motion are automatically derived by the SIMUUN computational tools.

B. Interaction with the Environment

Locomotion of an undulating body results from the coupling of its internal shape changes to external motion constraints, usually due to external frictional forces applied through the interaction with the locomotion environment, resisting the motion of body segments. In order to approximate the characteristics of this interaction, resistive force models have been developed, whereby the force on each link involves decoupled components in the normal and tangential direction of its motion (F_N and F_T, respectively), which depend on the corresponding link velocity components v_T and v_N. Use of such force models dates back to the analysis of anguilliform swimming in [18], variants of which have been applied to both aquatic and terrestrial locomotion. Assuming isotropic Coulomb-like interaction with the substrate, the resistive force components acting on the ith body link are obtained as $F_T^{Bi} = -\mu_T mg\,\mathrm{sgn}(v_T^{Bi})$ and $F_N^{Bi} = -\mu_N mg\,\mathrm{sgn}(v_N^{Bi})$, where m is the link's mass and g is the constant of gravity, while μ_T and μ_N are the tangential and normal Coulomb friction coefficients, respectively (Fig. 2). The latter depend on the configuration and material properties both of the links' contact surface and of the locomotion environment. In general, the larger the differential between these coefficients, the larger the stride length (distance traveled per undulation cycle) attainable for a given body wave. Moreover, the friction coefficients' ratio also determines, to a large extent, the direction of motion of the undulatory locomotor with respect to the body wave direction [1]. Most research efforts related to undulatory robots have considered the eel-like mode, which, for the friction model at hand, corresponds to $\mu_N/\mu_T \gg 1$, resulting in devices that achieve forward propulsion by head-to-tail body waves (e.g., [7]–[9], [13]–[16]). By contrast, when resistance in the tangential direction of link motion is higher than resistance in the normal direction (corresponding to $\mu_N/\mu_T < 1$), the overall locomotion is along the body wave direction, so that forward motion is by tail-to-head waves; we focus here on this polychaete-like mode of undulatory locomotion. It should be noted that, for the Coulomb model employed, when $\mu_N/\mu_T \simeq 1$, the system's resulting direction of motion also depends on the other system parameters.

Experiments with the robot parapodia moving on sand, detailed in Section V, indicated that the following simple Coulomb-like frictional force model $F_T^{Pj} = -f_T sgn(v_T^{Pj})$, $F_N^{Pj} = -f_N sgn(v_N^{Pj})$ is sufficient to describe the interaction of the jth parapodium with the specific environment (Fig. 2). The frictional coefficients f_N and f_T are determined experimentally.

III. MOTION CONTROL AND GAIT GENERATION

A. Pedundulatory Gait Generation

The pedundulatory mode of locomotion is based on the synergetic action of the body wave traveling along the mechanism, with appropriately coordinated movements of the parapodial appendages.

A traveling body wave can be generated in a serial chain of N links by having the $N-1$ joint angles vary sinusoidally, with a common amplitude A, frequency f, angular offset ψ and a constant phase lag ϕ_{lag} between consecutive joints. The time variation of the ith joint angle is:

$$\phi_i(t) = A\sin(2\pi f t + (N-i)\phi_{lag}) + \psi \;\;,\;\; i = 1,..,N-1 \tag{1}$$

This approach assumes full position control of the mechanism's joint angles. The propagation direction for the wave depends on the sign of the phase lag parameter, and is from link-1 to link-N for $\phi_{lag} > 0$. For $\psi = 0$, the locomotion of the mechanism is along a straight line, while curved paths are obtained for $\psi \neq 0$, where the resultant turning direction depends on the sign of both ψ and ϕ_{lag}, as well as on the type of environmental interaction (eel-like or polychaete-like).

The parapodial movements need to be appropriately coordinated with the body wave, in order to ensure their positive contribution in thrust generation during each periodic cycle of the system. In polychaete annelid worms, the alternating waves of parapodial activity are synchronized with the tail-to-head body undulations, so that the power stroke of each parapodium (when thrust is produced) occurs when the corresponding body segment is at the crest of the body wave, while its recovery phase occurs when the segment is in the trough of the body wave [4]–[6]. A straightforward way to achieve this with the mechanical system at hand (Fig. 2), involves the alternating activation of the right and left parapodium of the ith body segment as follows:

$$\chi_i = \begin{cases} A_p, & \text{for } s_i > r_i \\ 0, & \text{otherwise} \end{cases}, \quad \zeta_i = \begin{cases} A_p, & \text{for } s_i < -r_i \\ 0, & \text{otherwise} \end{cases}, \tag{2}$$

for $s_i = \sin(2\pi f t + (N + b/l - i)\phi_{lag})$, where the b/l term refers to the placement of the parapodia on the segment with respect to the joint (see Fig. 2), r_i is an appropriate threshold ($0 < r_i < 1$) and A_p is the parapodium joint angle amplitude, which should be sufficiently high to ensure that the parapodium penetrates the substratum.

Simulations of the robot "lifted in the air", i.e., in the absence of any external frictional forces (hence resulting

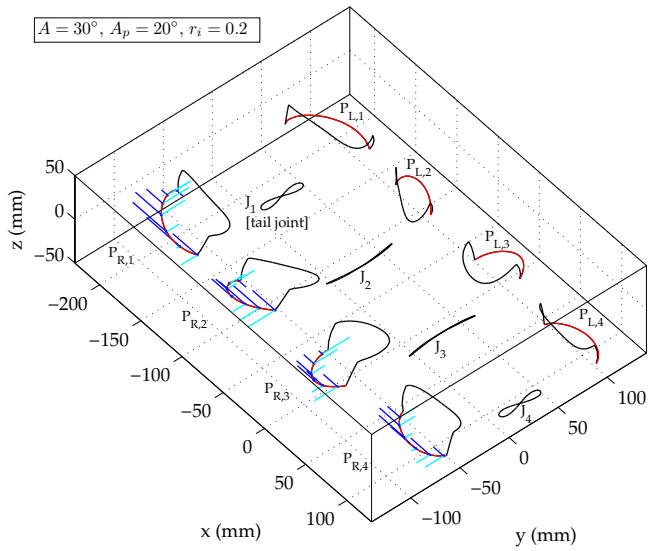

Fig. 3. Trajectories traced by the tips of all the parapodia in the Nereisbot model during a cycle of in-place pedundulation of the system. The part of the traces shown in red indicates the power stroke of the parapodia, when they are in contact with the substrate. The blue and cyan lines denote respectively the $x-$ and $y-$components of the parapodium velocity during the power stroke, indicating that the velocity is mostly directed towards the tail. The trajectories of the four body joints are also shown on the graph.

in in-place pedundulations of the system, without any net movement), indicate that the adopted control law (2) for the parapodia, when used in conjunction with a tail-to-head body wave (1), ensures that the parapodia move backwards relative to the substrate during their power stroke. Therefore, their contribution in thrust generation is, in general, positive when they are in contact with the ground (Fig. 3).

The parapodia provide a number of alternatives for instigating turning motions in pedundulatory systems. More specifically, the methods identified here are: (*a*) by introducing an angular offset $\psi \neq 0$ in the body wave (1), while the parapodia operate in the bilateral fashion described by (2), (*b*) by unilateral parapodial activations, while $\psi = 0$, and (*c*) by combining a non-zero angular offset with unilateral parapodial activation. The "unilateral" parapodial activation in these methods implies disabling all parapodial movement in the appropriate side of the mechanism, depending on the desired turning direction.

B. Simulation Studies of Pedundulatory Gaits

This section presents a series of SIMUUN simulations of the Nereisbot prototype, demonstrating pedundulatory locomotion by implementing the motion control strategies of the previous Section. The mechanical parameters (masses, dimensions, etc.) of the Nereisbot model developed in SIMUUN reflect those of the actual prototype. Appropriate frictional force measurements with the robot are used to select a plausible force model, for simulating the interaction of the body segments and of the parapodia, with the locomotion environment. This procedure is detailed in Section V, for experiments over fine sand, where the parameters of the models of Section II-B, are specified. In the simulations presented, Coulomb friction is used to model the interaction

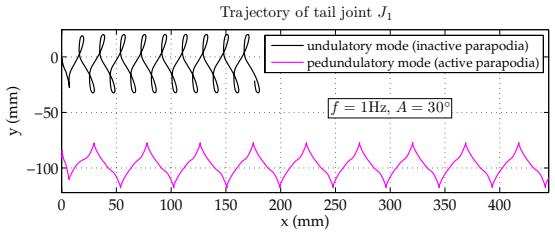

Fig. 4. Forward gait simulations of undulatory vs. pedundulatory locomotion (10 cycles shown for each).

of the body segments with the environment, with $\mu_T = 0.518$ and $\mu_N = 0.463$, while the coefficients of the parapodial frictional model are set to $f_N = 1.75\,\text{N}$ and $f_T = 0.06\,\text{N}$.

Using this setup, the pedundulatory gaits are implemented by (1)-(2), setting $\phi_{lag} = 2\pi/N$ in order to obtain a tail-to-head traveling wave whose wavelength equals the length of the mechanism. By disabling all of the system's parapodia, the purely undulatory gaits may be obtained, in order to draw comparisons regarding the locomotor efficiency of the proposed method. Indicative results for the forward gait are shown in Fig. 4, while Fig. 5 demonstrates the pedundulatory turning gaits identified previously.

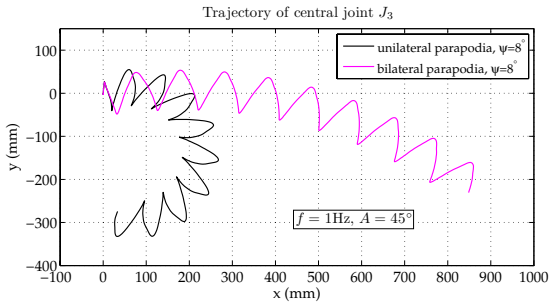

Fig. 5. Turning gait simulations of pedundulatory locomotion (10 cycles shown for each).

IV. PEDUNDULATORY ROBOTIC PROTOTYPES

In order to experimentally test the proposed locomotion strategy, a new 5-segment robotic prototype (Fig. 1b) has been developed, using off-the-shelf components and conventional fabrication techniques (see also [1]). It comprises four identical body segments, each equipped with a pair of parapodial appendages, and a conical head segment carrying the electronics. Each body segment (weight 270 g, length 100 mm, width 50 mm) has been fabricated from plastic and encases three motors, which actuate three rotary joints: a high-torque R/C servo unit (*HiTech* HSR-5995TG) drives the main body joint, through which consecutive segments are connected together, while a pair of smaller R/C servos (*HiTech* HS-81MG), placed on either side of the main body joint (Fig. 6a), are used to drive the segment's parapodia. The parapodia, which are directly mounted on the motor's shaft (Fig. 6b), so that their flat surface is lateral to the segment's main axis, are lightweight and capable of efficiently penetrating the substrate. The body segments' flat underside allows the attachment of different modules which

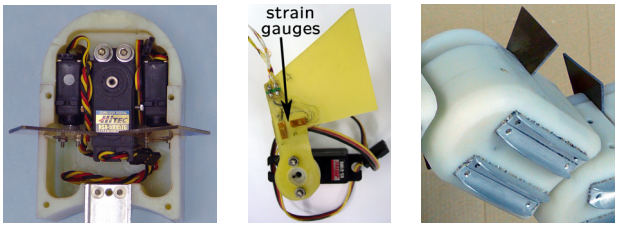

(a) (b) (c)

Fig. 6. Components of the Nereisbot prototype: (a) placement of the servo motors inside the body segments. (b) The instrumented parapodium, shown mounted on its motor. (c) The underside of a body segment, shown with two sets of longitudinally mounted blades.

implement the interaction with the locomotion environment, by providing differential friction in the tangential and normal directions of motion. For movement over relatively smooth surfaces, wheeled modules can be used. For movement over unstructured environments, such as sand, special modules have been developed (Fig. 6c), which employ aluminum blades whose number, spacing and orientation can be easily altered. The head segment has been shaped as a cone to aid the advancement through unstructured substrates, and carries the batteries powering the robot, as well as the on-board microcontroller unit (*Motorola* DSP56807), which generates all the control signals for the motors implementing the pedundulatory movements. Space restrictions prohibited fitting parapodia on this segment.

In addition, a special instrumented parapodium unit has been developed (Fig. 6b), which incorporates a set of four strain gauges (*Showa* N11-MA2-120-11) in a Wheatstone-bridge setup, appropriately configured to measure the normal component F_N^{Pj} of the force generated by the parapodium. The characteristic of the sensor was found, via calibration tests, to be linear in the operational range of interest.

This robotic prototype is versatile enough to allow the experimental study, not only of polychaete-like gaits, but of other, very different, pedundulatory gaits as well.

V. EXPERIMENTS ON SAND

Experimental results from tests, with the Nereisbot prototype moving over sand, are presented here and compared with the corresponding SIMUUN simulation results. Initial experiments (presented in Section V-A below) implement purely undulatory gaits by disabling all parapodial activity. This provides a comparative measure for evaluating the performance gains obtained by the pedundulatory mode. Experiments with the latter mode are presented in Section V-B.

Experimental setup: The prototype was placed inside a box (measuring 1.7 m x 1.7 m), which was uniformly filled with 35 mm of fine seashore sand (mean particle diameter: 0.6 mm). The experiments were conducted over a range of values for A ($20^\circ - 60^\circ$), with $f = 1$ Hz, and for two different configurations of the body segments' underside: (i) without blades, and (ii) with a total of four transversally mounted blades. A pair of colored markers was mounted on top of the tail (J_1) and central (J_3) joints of the mechanism.

TABLE I

FRICTION FORCE COEFFICIENTS.

	μ_T	μ_N	μ_T/μ_N
Without blades	0.518	0.463	1.111
Transversally mounted blades	0.852	0.741	1.150
Longitudinally mounted blades	0.741	0.926	0.800

These allowed the reconstruction of the respective joints' trajectories, via post-processing of the experiment videos.

In order to assess the developed computational models, corresponding simulations were carried out in SIMUUN, replicating for each experimental run the set of parameters used, and incorporating the frictional data below.

Frictional force measurements: In order to select an appropriate force model for the simulations, special measurements were performed to obtain data on the frictional characteristics of the mechanism, with respect to the configuration of the segments' underside (i.e., with or without blades) and the specific locomotion substrate. The forces required to move a single body segment over sand, in both the tangential and normal directions with respect to its main axis, were measured using a load cell. Much like the corresponding tests in [1], the interaction forces presented little variance in the range of traction velocities tested, indicating that a simple Coulomb friction model could be used for the interaction of the body with the sand environment. The resultant sets of Coulomb friction coefficients (summarized in Table I) indicate that, for the no-blade configuration, the resistance in the tangential direction is slightly higher than in the normal direction. The use of blades, despite significantly increasing the magnitude of the interaction forces (i.e., the resistance of the mechanism to motion), achieves only small increases in the friction differential μ_T/μ_N.

Due to their shape (cf. Fig. 6b) and movement, the tangential force component F_T^{Pj} of the parapodia is negligible with respect to the normal one F_N^{Pj}. A series of tests was performed with the instrumented parapodium mounted on the tail link of the mechanism, for the no-blades configuration. The measurements indicate that, for the specific parameters considered in (2), the movement of the parapodia is properly coordinated with the body wave, so that the forces imparted throughout the power stroke of each pedundulation cycle are positive (i.e., contributing to thrust generation). The average generated normal forces during the power stroke, for the

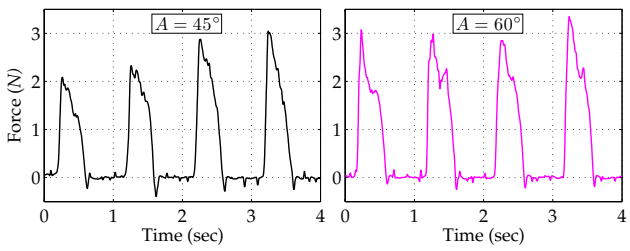

Fig. 7. Measurements of the normal force generated by the instrumented parapodium, placed at the mechanism's tail segment, during pedundulatory locomotion.

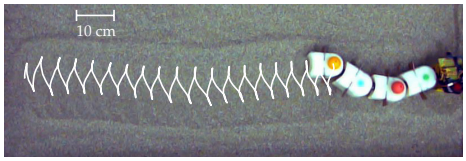

(a) no-blade configuration, A=60°

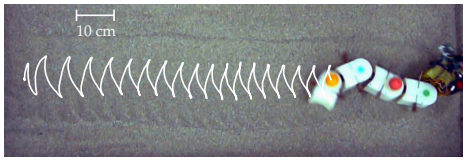

(b) transversal-blades configuration, A=60°

Fig. 8. Forward undulatory gait: Nereisbot experimental results. The traces show the trajectory of the tail joint J_1.

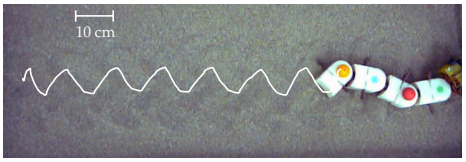

(a) no-blade configuration, A=60°

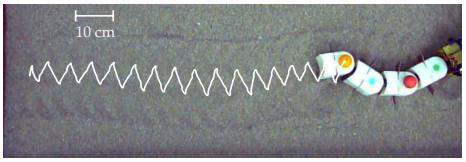

(b) transversal-blades configuration, A=60°

Fig. 10. Forward pedundulatory gait: Nereisbot experimental results. The traces show the trajectory of the tail joint J_1.

range of undulation amplitudes A tested, were found to be in the range $1.5-1.8$ N, demonstrating little dependence on the traction velocity. This validated our use of the Coulomb force model for the interaction of the parapodia with sand and specified appropriately the frictional coefficients. The measurement data also indicate a variance in the generated forces between successive pedundulation cycles. This could be attributed to the, possibly significant, variations in sand compaction and in the parapodium area submerged in the sand. Indicative force measurements are shown in Fig. 7.

A. Experiments of Undulatory Gait Generation

The experiments involving no parapodial activity demonstrated that the prototype is capable of advancing over the sandy terrain, via both forward and turning gaits, in the purely undulatory mode by a tail-to-head body wave. Indicative trajectories from forward gait experiments are shown in Fig. 8, and present considerable qualitative agreement with the results reported in [1]. The stride length S_L was found to increase with A, while there was little variation with respect to the use of friction blades (see Fig. 9). As in [1], our computational models were successful in capturing the main aspects of the body undulations, as the simulation-derived plots for S_L show considerable qualitative and quantitative agreement with the experimentally obtained ones.

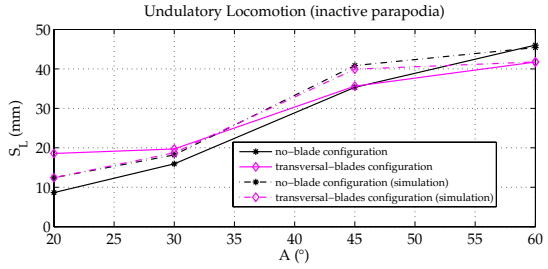

Fig. 9. Forward undulatory gait: experimental (solid lines) vs. simulation-derived (dashed lines) stride length estimates.

B. Experiments of Pedundulatory Gait Generation

The main set of experiments, related to pedundulatory gait generation, was carried out by setting the threshold parameter in (2) to $r_i = 0.2$ for all four parapodia pairs of the mechanism. Indicative results, and the associated stride lengths, are shown in Figs. 10-11, illustrating the increased performance afforded by the use of parapodia, in addition to the tail-to-head body undulations. It is noteworthy that, unlike the purely undulatory mode, there is a significant difference in the overall performance with regard to the configuration of the mechanism's underside: although the transversal-blade configuration does demonstrate moderate gains from the use of parapodia, it is the no-blade configuration that presents the most pronounced increase in the attained stride length, which reaches values exceeding 130 mm.

The SIMUUN computational models appear to capture adequately the experimental observations, especially in the case of the no-blades configuration (Fig. 11).

The different methods for obtaining turning motions with the pedundulatory system, identified in Section III, have also been experimentally validated (Fig. 12). The effect of the angular offset ψ on the turning direction and turning radius of the system's trajectory is illustrated in Fig. 12(d).

C. Discussion

Pedundulatory locomotion increases the attained stride length S_L, and thus the velocity $v = fS_L$ of the robot, as is evident by comparing Figs. 9 and 11. Increasing the body joint angle amplitude A (in the examined range of $20°-60°$) increases, almost linearly, the stride length and the corresponding velocity. The maximum velocity of the robot in purely undulatory mode was approximately 0.17 km / h, while the maximum velocity attained in pedundulatory mode was approximately 0.5 km / h, i.e., three times higher.

A similar increase in stride length was also observed in

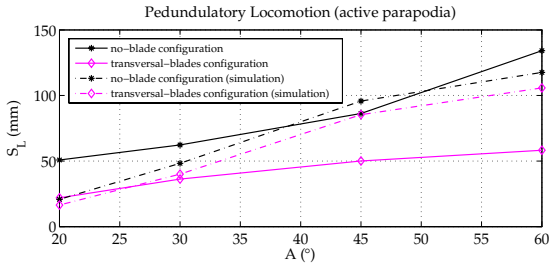

Fig. 11. Forward pedundulatory gait: experimental (solid lines) vs. simulation-derived (dashed lines) stride length estimates.

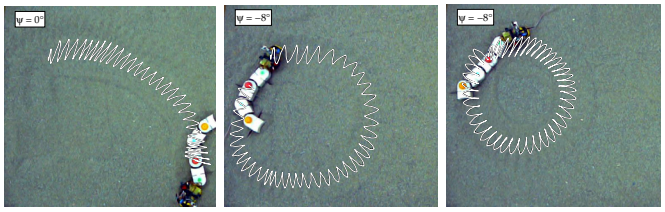

(a) unilateral parapodia activation (b) bilateral parapodia activation (c) unilateral parapodia activation

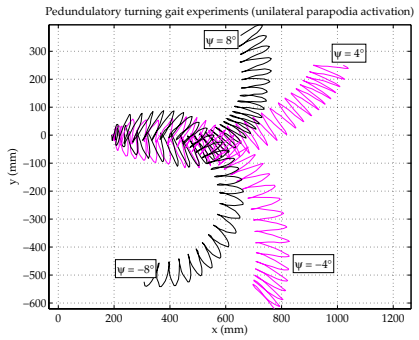

(d) unilateral parapodia activation: effect of joint angle offset ψ

Fig. 12. Turning pedundulatory gait: experimental results for the no-blade configuration. The traces show the trajectory of the central joint J_3.

turning gaits (Fig. 12). These results reveal multiple possible strategies of exploiting parapodia, giving rise to several distinct locomotor patterns.

The modeling of the interaction of our robot with sand does not take into account the shifting of the substrate material during robot locomotion. Shaping the robot segments as in the present prototype and avoiding the use of blades, reduces, but does not eliminate, the movement, even the compaction, of the sand. This sand movement strains the robot actuators, and may affect adversely their capability to implement a desired joint trajectory, while it creates tracks which may bias the robot trajectory. Moreover, it could be at the origin of the reduced performance of the transversal-blades configuration, compared to the no-blades one, during the forward pedundulatory gait. It is noteworthy, however, that the parapodia appear to greatly enhance the locomotion capabilities of the robot under these conditions.

Burrowing: A common activity of polychaete annelids is terrain manipulation, in particular burrowing. In order to explore such capabilities of our robot, several forward locomotion experiments were performed with the mechanism covered almost entirely with sand: the robot was still easily able to move forward, albeit at a reduced speed, demonstrating the potential of both the tail-to-head body undulations and of the parapodia for burrowing tasks. A more detailed investigation of this capability would be of interest.

VI. CONCLUSIONS

This paper considers biomimetic robots inspired from the morphology and locomotion strategy of the polychaete annelid marine worms, and studies, both experimentally and in simulation, the combination of parapodial and undulatory locomotion (which we term here pedundulatory locomotion) for such robots on sand. These studies demonstrate the efficiency of this mode of locomotion on sand, compared to purely undulatory locomotion. Apart from the results presented here, evidence was obtained during these experiments that this class of robotic locomotors displays a rich variety of gaits (including centipede-like gaits [5]), significant burrowing capabilities, and performs well on different types of sand and pebbles, for different robot morphologies and sizes.

Future work will further investigate pedundulatory locomotion, will extend our computational models to describe more accurately locomotion on sand and on other unstructured substrates (mud, gravel, etc.), and will explore the generation of corresponding reactive behaviors [2], [3].

VII. ACKNOWLEDGMENTS

The authors thank P. Georgiades and N. Pateromichelakis for their technical assistance. Related papers and videos can be found at the Web site *www.ics.forth.gr/~tsakiris*

REFERENCES

[1] D.P. Tsakiris, M. Sfakiotakis, A. Menciassi, G. La Spina, and P. Dario, "Polychaete-like undulatory robotic locomotion," in *Proc. IEEE Int. Conf. on Robotics and Automation (ICRA'05)*, Barcelona, Spain, 2005, pp. 3029–3034.

[2] M. Sfakiotakis, D.P. Tsakiris, and A. Vlaikidis, "Biomimetic centering for undulatory robots," in *Proc. 1st IEEE/RAS-EMBS Int. Conf. on Biomedical Robotics and Biomechatronics (BIOROB'06)*, Pisa, Italy, 2006, pp. 744–749.

[3] M. Sfakiotakis and D.P. Tsakiris, "Neuromuscular control of reactive behaviors for undulatory robots," *Neurocomputing*, (in press), *doi:10.1016/j.neucom.2006.10.139*.

[4] J. Gray, "Annelids," in *Animal Locomotion*. London: Weidenfeld & Nicolson, 1968, pp. 377–410.

[5] R. Brusca and G. Brusca, *Invertebrates*. Sunderland: Sinauer Associates, 1990.

[6] R. Clark and D. Tritton, "Swimming mechanisms in nereidiform polychaetes," *J. Zool.*, vol. 161, pp. 257–271, 1970.

[7] S. Hirose, *Biologically Inspired Robots: Snake-Like Locomotors and Manipulators*. New York: Oxford University Press, 1993.

[8] S. Hirose and E. Fukushima, "Snakes and strings: New robotic components for rescue operations," *Int. J. Robot. Res.*, vol. 23, no. 4/5, pp. 341–349, 2004.

[9] J. Ostrowski and J. Burdick, "The geometric mechanics of undulatory robotic locomotion," *Int. J. Robot. Res.*, vol. 17, no. 7, pp. 683–701, 1998.

[10] S. Ma, "Development of a creeping locomotion snake-robot," *Int. J. Robot. Automat.*, vol. 17, no. 4, pp. 146–153, 2002.

[11] P.S. Krishnaprasad and D.P. Tsakiris, "Oscillations, SE(2)-snakes and motion control: A study of the roller racer," *Dyn. Syst.*, vol. 16, no. 4, pp. 347–397, 2001.

[12] M. Nilsson, "Serpentine locomotion on surfaces with uniform friction," in *Proc. IEEE/RSJ Int. Conf. on Intelligent Robots and Systems (IROS'04)*, Sendai, Japan, 2004, pp. 1751–1755.

[13] M. Saito, M. Fukaya, and T. Iwasaki, "Modeling, analysis, and synthesis of serpentine locomotion with a multilink robotic snake," *IEEE Control Syst. Mag.*, vol. 22, no. 1, pp. 64–81, 2002.

[14] A. Ijspeert, A. Crespi, and J. Cabelguen, "Simulation and robotics studies of salamander locomotion. Applying neurobiological principles to the control of locomotion in robots," *Neuroinf.*, vol. 3, no. 3, pp. 171–196, 2005.

[15] S. Kelly and R. Murray, "Modelling efficient pisciform swimming for control," *Int. J. Robust Nonl. Contr.*, vol. 10, no. 4, pp. 217–241, 2000.

[16] J. Cortes, S. Martinez, J. Ostrowski, and K. McIsaac, "Optimal gaits for dynamic robotic locomotion," *Int. J. Robot. Res.*, vol. 20, no. 9, pp. 707–728, 2001.

[17] M. Sfakiotakis and D.P. Tsakiris, "SIMUUN: A simulation environment for undulatory locomotion," *Int. J. Model. Simul.*, vol. 26, no. 4, pp. 4430–4464, 2006.

[18] G. Taylor, "Analysis of the swimming of long and narrow animals," *Proc. R. Soc. Lond. Ser. A*, vol. 214, pp. 158–183, 1952.